Volume 2 | Number 8 | August 2015

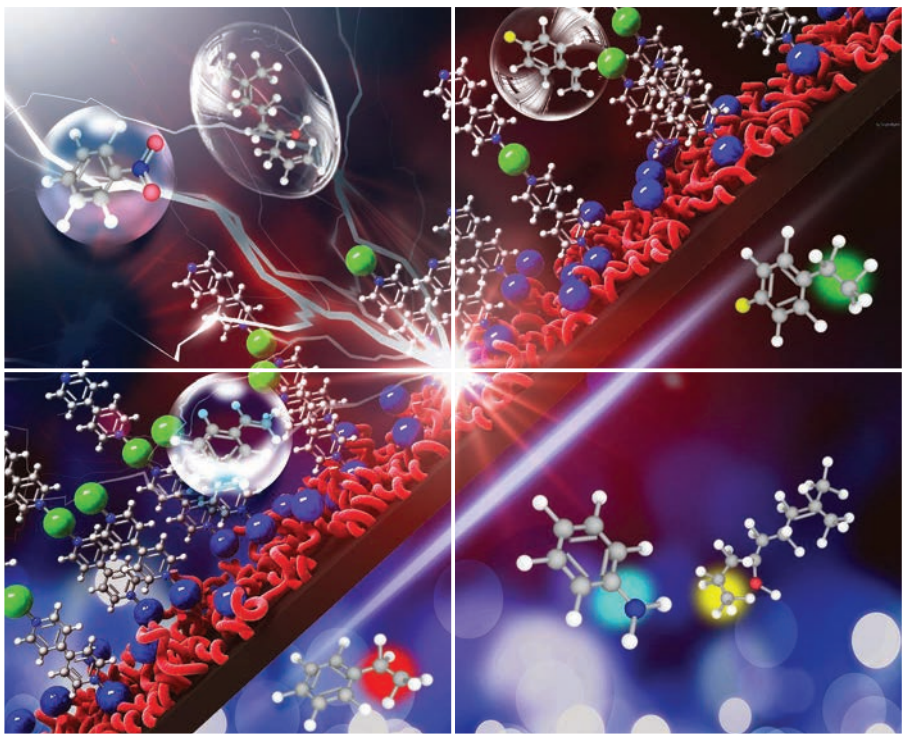

INORGANIC CHEMISTRY

FRONTIERS

Chinese Chemical Society
PEKING UNIVERSITY 1898
ROYAL SOCIETY OF CHEMISTRY

http://rsc.li/frontiers-inorganic

INORGANIC CHEMISTRY
FRONTIERS

RESEARCH ARTICLE

Cite this: *Inorg. Chem. Front.*, 2015, **2**, 749

A Ni(II) dinuclear complex bridged by end-on azide-N and phenolate-O atoms: spectral interpretation, magnetism and biological study†

Kuheli Das,[a] Amitabha Datta,*[b] Soumendranath Nandi,[a] Sandeep B. Mane,[b] Sudipa Mondal,[a] Chiara Massera,[c] Chittaranjan Sinha,*[a] Chen-Hsiung Hung,*[b] Tulin Askun,[d] Pinar Celikboyun,[d] Zerrin Cantürk,[e] Eugenio Garribba[f] and Takashiro Akitsu[g]

A potential tetradentate monoanionic N_2O_2 chelator, HL, derived from the condensation of *o*-vanillin and *N,N*-dimethylethylenediammine, has been reacted with nickel perchlorate and sodium azide to yield the dinuclear Ni(II) complex $[Ni(L)(\mu_{1,1}\text{-}N_3)Ni(L)(OH_2)_2]\cdot ClO_4$ (**1**), where L = $Me_2N(CH_2)_2N{=}CH{-}C_6H_3(O^-)\text{-}(OCH_3)$. The complex has been characterized by X-ray diffraction analysis and different spectroscopic techniques. The coordination geometry around the Ni(II) centres is a distorted octahedron, with the azide ligand and the phenolato oxygen atom bridging in $\mu_{1,1}$ and μ_2 mode, respectively. The EPR spectra, recorded at liquid nitrogen temperature (77 K) and room temperature (298 K), show *g* factors of 2.080 and 2.085, in agreement with the structure determined by X-ray diffraction analysis. The VTM study confirms that there are ferromagnetic interactions between the bridging binuclear Ni(II) ions (S = 1). The evaluation of cytotoxic effects on different human cancer cell lines (A-549, MCF-7 and CaCo-2) suggests that both the ligand and complex **1** have potential anticancer properties. Furthermore, they also exhibit anti-mycobacterial activity against *M. tuberculosis* H37Rv (ATCC 27294) and *M. tuberculosis* H37Ra (ATCC 25177) strains. Molecular docking of HL with the enoyl acyl carrier protein reductase of *M. tuberculosis* $H37R_v$ (PDB ID: 4U0K) has been examined, showing that HL forms two hydrogen bonds with Lys165 (1.94 and 2.53 Å) in its best docked pose.

Received 11th April 2015,
Accepted 12th June 2015

DOI: 10.1039/c5qi00060b

rsc.li/frontiers-inorganic

Introduction

Metal complexes containing Schiff-base ligands derived from aromatic carbonyl compounds have been widely studied in connection with metallo-protein models because of the versatility of their steric and electronic properties, which can be fine-tuned by choosing the appropriate amine precursors and ring substituents.[1] It has been recognized that the metal centres and the binding Schiff base ligands (as anions or capping molecules) may play important roles in the formation of desirable compounds, due to their different molecular shapes, charge and sizes.[2] Besides, coligands can also be used to tune the properties of the resulting compounds. Several pseudohalide-bridged metal complexes with various Schiff bases continue to be a subject of much interest, and intensive investigations have taken place to shed light on their diverse structures and potential applications as magnetic materials.[3] Among the pseudohalides, the azido group has received much attention due to its versatility as a bridging ligand and due to the wide variety of magnetic properties shown by its compounds. The versatile azide ion, which can indeed form dimers, clusters, and polymers exhibiting significant magnetic properties such as ferro- and antiferromagnetic interactions, has been extensively used because it may induce interesting magnetic couplings by two different bonding modes, *i.e.* end-

[a]*Department of Chemistry, Jadavpur University, Kolkata 700032, India. E-mail: c_r_sinha@yahoo.com*
[b]*Institute of Chemistry, Academia Sinica, Taipei 115, Taiwan. E-mail: amitd_ju@yahoo.co.in, chhung@gate.sinica.edu.tw*
[c]*Dipartimento di Chimica, Università degli Studi di Parma, Viale delle Scienze, 17/A, 43124 Parma, Italy*
[d]*Department of Biology, Faculty of Sciences and Arts, University of Balikesir, Cagis Campus, 10145 Balikesir, Turkey*
[e]*Department of Pharmaceutical Microbiology, Pharmacy Faculty, Anadolu University, Yunusemre Campus, 26470 Eskisehir, Turkey*
[f]*Dipartimento di Chimica e Farmacia, and Centro Interdisciplinare per lo Sviluppo della Ricerca Biotecnologica e per lo Studio della Biodiversità della Sardegna, Università di Sassari, Via Vienna 2, I-07100 Sassari, Italy*
[g]*Department of Chemistry, Faculty of Science, Tokyo University of Science, 1-3 Kagurazaka, Shinjuku-ku, Tokyo 162-8601, Japan*
†Electronic supplementary information (ESI) available. CCDC 894363. For ESI and crystallographic data in CIF or other electronic format see DOI: 10.1039/c5qi00060b

on ($\mu_{1,1}$ ferromagnetic) and end-to-end ($\mu_{1,3}$ antiferromagnetic).[4] It is worth reporting that the ferromagnetic ordering between the metal centres induced by the end-on or 1,1-coordination mode is reduced if the bridging bite angle exceeds 108°.[5] The chemistry of nickel complexes with multidentate Schiff base ligands has also attracted great attention; indeed, magnetic exchange interactions between metal centres in binuclear nickel salts continue to be a subject of wide interest, with particular emphasis on determining magnetic structural correlations.[6] Many structural parameters affect the superexchange mechanism in these sorts of dimers.[7] Kahn[8] has suggested that the exchange integral is the sum of two antagonistic interactions favoring the antiferromagnetic and ferromagnetic interactions.

Nickel complexes play an important role in bioinorganic chemistry and may provide the basis of models for active sites of biological systems or act as catalysts.[9] Tuberculosis, an infectious and chronic bacterial disease, caused primarily by the bacillus *Mycobacterium tuberculosis* and rarely by *M. bovis* and *M. africanum*, affects the lung (pulmonary TB) and can even spread to the other organs (extrapulmonary TB).[10] Millions of children die every year from this disease.[11] Mycobacteria are resistant (multidrug resistant or MDR-TB) to many chemicals, disinfectants, antibiotics and chemo-therapeutical agents.[12] Synthetic chemistry research is now directed to exploring the synergistic relationships between natural products and synthetic drugs for better treatment. Cytotoxicity assays are widely used in bio-inorganic chemistry to screen for cytotoxicity in compound libraries. Assessing cell membrane integrity is one of the most common ways to measure cell viability and cytotoxic effects. The control of tumor cell proliferation by inhibition of the cell cycle and induction of apoptosis could provide a therapeutic strategy for the treatment of cancer.[13] Programmed cell death plays an important role in the regulation of cellular homeostasis.[14] Marin-Hernandez *et al.*[15] indicated that some mixed chelate transition metal-based drugs have more potent antitumor activity than cisplatin in *in vivo* and *in vitro* studies of a variety of tumor cells. However, human cancer cell lines are a useful model to study cell growth inhibition of tumor cells by natural compounds or newly synthesized compounds.

Recently, a unique example of bridge distance dependency of the exchange interaction has emerged from the magnetic properties of a μ-phenoxo-$\mu_{1,1}$-N_3 dinickel(II) compound.[16] In our present contribution, we report the structural description and DFT computation analysis of the Ni(II) derivative $[Ni(L)(\mu_{1,1}\text{-}N_3)Ni(L)(OH_2)_2]\cdot ClO_4$ (**1**), where L = $Me_2N(CH_2)_2N{=}CH\text{–}C_6H_3(O^-)(OCH_3)$;[17] additionally, the spectral properties and temperature-dependent magnetic behaviour of the complex are elucidated. Both the ligand HL and complex **1** exhibit antimycobacterial activity on *M. tuberculosis* H37Rv (ATCC 27294) and *M. tuberculosis* H37Ra (ATCC 25177) strains. The antimycobacterial efficiency of HL has been examined by molecular docking with the enoyl acyl carrier protein reductase of *M. tuberculosis* $H37R_v$ (PDB ID: 4U0K) and has been compared with the first line drug isoniazide.

Experimental

Materials

o-Vanillin and 2-dimethylaminoethylamine (Merck) and sodium azide (Sigma-Aldrich) were purchased and used as received without further purification. Hydrated nickel(II) perchlorate was prepared by treatment of nickel(II) carbonate basic hydrate, $NiCO_3\cdot 2Ni(OH)_2$ (AR grade, E. Merck), with perchloric acid (AR grade, E. Merck), followed by slow evaporation on a steam bath. It was then filtered through a fine glass frit and stored in $CaCl_2$ desiccators. All the solvents used were of reagent grade. The ligand (HL) synthesis was carried out following a published procedure.[17]

Physical measurements

Microanalytical data (C, H, and N) were collected on a Perkin-Elmer 2400 CHNS/O elemental analyzer. FTIR spectra were recorded on a Perkin-Elmer RX-1 spectrophotometer in the range 4000–400 cm^{-1} with KBr pellets. Electronic spectra were recorded on a Lambda 25 (UV–Vis–NIR) spectrophotometer in methanol. Emission spectra were examined with an LS 55 Perkin-Elmer spectrofluorometer at room temperature (298 K) in different solutions under degassed conditions. The fluorescence quantum yield of the complexes was determined using carbazole as a reference with a known Φ_R of 0.42 in benzene.[18] The complex and the reference dye were excited at the same wavelength, maintaining a nearly equal absorbance (~0.1), and the emission spectra were recorded. The area of the emission spectrum was integrated using the software available in the instrument and the quantum yield was calculated according to the following equation:

$$\frac{\phi_S}{\phi_R} = \left[\frac{A_S}{A_R}\right] \times \left[\frac{(Abs)_R}{(Abs)_S}\right] \times \left[\frac{{\eta_S}^2}{{\eta_R}^2}\right]$$

Here, Φ_S and Φ_R are the fluorescence quantum yield of the sample and reference, respectively. A_S and A_R are the area under the fluorescence spectra of the sample and the reference, respectively, $(Abs)_S$ and $(Abs)_R$ are the respective optical densities of the sample and the reference solution at the wavelength of excitation, and η_S and η_R are the values of the refractive index for the respective solvent used for the sample and reference.[19] EPR spectra were recorded from 0 to 10 000 Gauss in the temperature range 77–298 K with an X-band (9.4 GHz) Bruker EMX spectrometer equipped with an HP 53150A microwave frequency counter. Magnetic properties were investigated with a Quantum Design MPMS-XL superconducting quantum interference device magnetometer (SQUID) at an applied field of 10 000 Oe in the temperature range 5–300 K. Diamagnetic correction was carried out by using Pascal constants.

Synthesis of the ligand, HL

The ligand, HL, 2-[{[2-(dimethylamino)ethyl]imino}methyl]-6-methoxyphenol, was prepared[17] by condensation of *o*-vanillin (0.152 g, 1.0 mmol) with 2-dimethylaminoethylamine (0.109 ml, 1 mmol) in methanol (15 mL). After 2 h reflux, the

pale yellow methanolic solution was cooled down to room temperature. The solvent was removed under reduced pressure, and the Schiff-base ligand was obtained as a light-yellow liquid that was used without further purification. ^{1}H NMR (TMS, $CDCl_3$) δ: 12.80 (1H, s, H-1,), 9.90 (1H, s, H-6,6′), 6.46–6.86 (3H, d & t, Ar-H), 3.86 (3H, s, H-6), 3.45 (2H, t, J = 4.5 Hz, H-7), 3.72 (2H, t, J = 3.4 Hz, H-8), 2.29 (6H, s, H-9) ppm (see ESI, Fig. S1†).

Synthesis of the complex (1)

Upon the addition of HL (1 mmol) in methanol (20 mL) to Ni-$(ClO_4)_2{\cdot}6H_2O$ (0.36 g, 1 mmol) in the same solvent the mixture was stirred for half an hour and then a solution of NaN_3 (0.03 g, 0.5 mmol) in the minimum volume of water was added, and the reaction mixture was kept undisturbed and allowed to evaporate slowly. After ten days, dark brown, rectangular-shaped single crystals of **1** were obtained. The crystals were filtered off, washed with water and dried in air. Yield: 71%. Anal. Calc. for $C_{24}H_{42}Ni_2N_7O_{12}Cl$: C, 37.23; H, 5.47; N, 12.67. Found: C, 37.73; H, 5.09; N, 12.83%.

X-ray crystallography

The crystal structure of complex **1** was determined by X-ray diffraction methods. Crystal data and experimental details for data collection and structure refinement are reported in Table 1. Intensity data and cell parameters were recorded at 293(2) K on a Bruker Breeze (MoKα radiation = 0.71069 Å) equipped with a CCD area detector and a graphite monochromator. No significant crystal decay was observed. The raw frame data were processed using SAINT and SADABS to yield the reflection data file.[20] The structure was solved by direct methods using the SIR97 program[21] and refined on F_o^2 by full-matrix least-squares procedures, using the SHELXL-97 program[22] in the WinGX suite v.1.80.05.[23] All non-hydrogen atoms were refined with anisotropic atomic displacements with the exception of the oxygen atoms of the perchlorate ion and the oxygen atoms of the lattice water molecules. The hydrogen atoms were included in the refinement at idealized geometry (C–H 0.95 Å) and refined "riding" on the corresponding parent atoms. The weighting scheme used in the last cycle of refinement was $w = 1/[\sigma^2F_o^2 + (1016)^2]$, where $P = (F_o^2 + 2F_c^2)/3$. Crystallographic data (excluding structure factors) for the structure reported have been deposited with the Cambridge Crystallographic Data Centre as supplementary publication no. CCDC 894363.

Table 1 Crystallographic data of complex **1**

Empirical formula	$C_{24}H_{42}ClN_7O_{12}Ni_2$
Formula weight	773.52
Temperature	293(2)
Wavelength (Å)	0.71069
Crystal system	Monoclinic
Space group	*P*21
a, Å	11.748(2)
b, Å	11.093(1)
c, Å	13.278(2)
β, °	100.963(2)
Volume, Å^3	1698.8(4)
Z	2
$D_{calc.}$ (mg m^{-3})	1.512
μ (Mo Kα) (mm^{-1})	1.254
F(000)	808
θ range for data collection	1.56–28.34
Reflections collected/unique	24 015/8462 [R(int) = 0.0416
Observed reflections [$F_o > 4\sigma(F_o)$]	5861
Data/restraints/parameters	8462/4/390
Goodness-of-fit on F^2 [a]	0.991
Final R indices [$F_o > 4\sigma(F_o)$][b]	R_1 = 0.0543, wR_2 = 0.1408
R indices (all data)	R_1 = 0.0882, wR_2 = 0.1641
Largest diff. peak and hole, e Å^{-3}	0.687 and −0.663

[a] Goodness-of-fit $S = [\sum w(F_o^2 - F_c^2)^2/(n-p)]1/2$, where n is the number of reflections and p is the number of parameters. [b] $R_1 = \sum||F_o| - |F_c||/\sum|F_o|$, $wR_2 = [\sum[w(F_o^2 - F_c^2)^2]/\sum[w(F_o^2)^2]]^{1/2}$.

Theoretical calculations

Full geometry optimization of **1** and **2** was carried out using density functional theory (DFT) at the B3LYP level.[24] All calculations were performed using the Gaussian 03 program package[25] with the aid of the Gauss View visualization program.[26] For C, H, N, O, and Cl the 6-31G(d) basis set was assigned, while for Cu and Ni the LanL2DZ basis set with effective core potential was employed.[27] The vibrational frequency calculations were performed to ensure that the optimized geometries represent the local minima and there are only positive eigenvalues. Vertical electronic excitations based on B3LYP optimized geometries were computed using the time-dependent density functional theory (TD-DFT) formalism[28–30] in acetonitrile using the conductor-like polarizable continuum model (CPCM).[31] Gauss sum was used to calculate the fractional contributions of various groups to each molecular orbital.[32]

Anti-mycobacterial activity

Microorganisms. In the antimycobacterial assay, *M. tuberculosis* $H_{37}Rv$ (ATCC 27294), *M. tuberculosis* $H_{37}Ra$ (ATCC 25177) strains and two clinical strains (strain-1 and strain-2) obtained from the hospital were used.

Medium. In the assays, Mycobacteria Growth Indicator Tubes (MGIT) and their supplements, BBL MGIT OADC enrichment and BBL MGIT PANTA, were purchased from BD. The MGIT contains 4 mL of modified Middlebrook 7H9 Broth base.

Inoculum preparation. For the cultivation of mycobacteria, the MGIT (Mycobacteria Growth Indicator Tube), a fluorescent compound, is embedded in silicone on the bottom, and then 4 mL of modified Middlebrook 7H9 Broth base are added to the mixture. After that, 0.5 mL of OADC enrichment (an oleic acid, albumin, dextrose and catalase) and PANTA antibiotic mixture to prevent the proliferation of any non-mycobacteria (0.1 mL) are added to this medium. Tubes are incubated at 37 °C. For the positive control, MGIT tubes are prepared by inoculating bacteria, and tube reading was started on the second day of incubation using a Micro MGIT fluorescence reader which uses long wavelength UV light.[33] To prepare the inoculum the positive tubes (day 1 or day 2 positive) are used

directly as inoculums. The positive tubes between day 3 and day 5 are diluted to 1 : 4 ratio using sterile saline. Inoculums, prepared from a day 1 to day 5 MGIT 7 mL positive tube, range between 0.8×10^5 and 3.2×10^5 CFU per mL. Each assay is performed according to the MGIT manual fluorometric susceptibility test procedure recommended by the manufacturer.[33,34]

Antimycobacterial susceptibility assay. The activity of the ligand, HL, and complex **1** against *M. tuberculosis* strains was tested using the Microplate Presto Blue Assay (MPBA) by the method described by Collins & Franzblau[35] and modified by Jimenez-Arellanes *et al.*[36] 100 μl of the compound was transferred to the first column; then 100 μl of 7H9 broth was transferred from column 1 to column 10. Columns 11 and 12 were negative and positive controls respectively. 100 μl of the compound were transferred from column 1 to column 2. Then it was mixed using pipettes three times; the procedure was repeated to provide serial 1 : 2 dilutions. 100 μl of excess medium was discarded from the wells in column 10. Final test concentration ranges were 512–1 μg ml^{-1} in the mixture. Microplates were inoculated with the bacterial suspension (20 μL per well) except for the negative control and incubated at 37 °C for 6 days. Presto blue (15 μL, Life Technologies) was then added to the bacterial growth control wells (without compound) and the microplates were incubated at 37 °C for an additional 24 h. If the dye turned from blue to pink/red (indicating positive bacterial growth), the Presto blue solution was added to the other wells to determine the MIC values. All tests were performed in triplicate. The minimal inhibitory concentration (MIC) was defined as the lowest concentration of the sample that prevents a colour change to pink/red. To determine the minimal bactericidal concentration (MBC) values, MIC concentration-wells and higher concentration wells were used. To each well it was transferred fresh 7H9 broth (185 μL) and added a mycobacterial suspension (15 μL). Plates were incubated at 37 °C for 6 days. The MBC corresponded to the minimum compound concentration which does not cause a colour change in the cultures when re-incubated in fresh medium.[37] Streptomycin (STR), ethambutol (EMB), rifampicin (RFP) and isoniazid (INH) were used as standard drugs.

Cytotoxicity study

Cell culture. A-549 (non-small cell lung cancer), MCF-7 (breast cancer), Caco-2 (colon cancer cell line) and healthy cell lines, CRL-2522 (human normal fibroblast), were used in the study, provided by ATCC cell bank. The cells were grown in RPMI 1640 medium supplemented with 2 mM L-glutamine, 10% fetal bovine serum, and 1% penicillin–streptomycin at a temperature of 37 °C in a humidified incubator under a 5% CO_2 atmosphere.

Cell viability test by the MTT assay. The MTT [3-(4,5-dimethylthiazol-2-yl)-2,5-diphenyl tetrazolium bromide] assay was performed to determine the effect of the ligand, HL, and complex **1**; the following concentrations (500, 250, 125, 62.5, 31.25, 15.625, 7.8125, 3.9, 1.95, 0.97 μg ml^{-1}) were seeded on 5×10^3 cells which were cultivated in each well of the plate with 96 wells. After 24 hours of incubation, 0.1 ml MTT working solution (0.5 mg mL^{-1}) was added to each well and they were incubated at 37 °C in a 5% CO_2 incubator for 3–4 hours. After that, the unreacted dye was removed and the insoluble formazan crystals[38] were dissolved in DMSO. The absorbance intensity of the living cells on the plate was measured in an ELISA device (Cytation3, Biotek, USA) at 540 nm. The acquired absorbance values corresponded to metabolic activities in the cells in culture media. Because this value was correlated with the number of living cells, the results were expressed in liveliness percent and calculated using the formula below:

$$\text{Liveliness percent} = \frac{100}{\text{Absorbance of the control}/\text{Absorbance of the sample}}$$

Docking studies

Molecular docking is used to predict how a protein interacts with small molecules. The crystal structure of the enoyl acyl carrier protein reductase of *M. tuberculosis* $H37R_v$ was downloaded from the RCSB protein data bank (http://www.pdb.org) and used for docking. The protein (PDB id: 4U0K) was co-crystallized with (3*S*)-*N*-(5-chloro-2-methylphenyl)-1-cyclohexyl-5-oxopyrrolidine-3-carboxamide and nicotinamide-adenine-dinucleotide. *In silico* docking studies were performed using the CDOCKER module of the Receptor–Ligand interactions protocol section of Discovery Studio client 3.5.[39] Initially there was a pre-treatment process for the protein and the ligand. The structure of the ligand was drawn in Chemdraw 5.0, saved as a .mol file and finally the .mol file was imported to the Discovery Studio 4.0 platform. The ligand preparation was done using the Prepare Ligand module in the Receptor–Ligand interactions tool of Discovery Studio 4.0 and the prepared ligand was hence used for docking. The protein preparation was done using the Prepare Protein module of the Receptor–Ligand interactions tool of Discovery Studio 4.0 and that was used for docking. We subsequently defined the protein as the total receptor and the active site was selected based on the ligand binding domain of (3*S*)-*N*-(5-chloro-2-methylphenyl)-1-cyclohexyl-5-oxopyrrolidine-3-carboxamide and nicotinamide-adenine-dinucleotide. Then the pre-existing ligand was removed and the prepared ligand was placed instead. The most favourable docked pose was selected according to the minimum free energy of the protein–ligand complex and analysed to investigate the interaction.

ADMET prediction

Absorption, distribution, metabolism, excretion and toxicity (ADMET) predictions were done using the ADMET descriptor module of the Small molecules protocol of Discovery Studio client 4.0. Also the druglikeness of the compounds was checked following Lipinski's rule of five.[40,41]

Results and discussion

Synthesis and formulation

The monoanionic Schiff base precursor [2-[{[2-(dimethylamino)ethyl]imino}methyl]-6-methoxyphenol] (HL) was prepared by the condensation of *o*-vanillin and *N*,*N*-dimethylethylenediammine (1 : 1 mole proportion) in methanol. HL was then reacted with $Ni(ClO_4)_2{\cdot}6H_2O$ and NaN_3 in a methanol/water mixture to yield $[Ni(L)(\mu_{1,1}\text{-}N_3)Ni(L)(OH_2)_2]{\cdot}ClO_4$ (**1**), where L = $Me_2N(CH_2)_2N{=}CH{-}C_6H_3(O^-)(OCH_3)$, by slow evaporation of the solvent. The ^1H NMR spectrum of HL shows singlet signals at δ 12.80 and 9.90 ppm for –OH and –CH=N protons, respectively. Furthermore, the singlet signals at δ 3.86 ppm and 2.29 ppm refer to $-OCH_3$ and $-N(CH_3)_2$ protons, respectively. In addition, two triplet signals at δ 3.45 and 3.07 ppm are assigned to 7-H and 8-H protons with *J* values of 4.5 and 3.4 Hz respectively. The corresponding aromatic protons appear as doublet and triplet signals in the region 6.46–6.86 ppm. The FTIR spectrum of the free ligand shows bands at 3436 cm^{-1} and 1660 cm^{-1} which are due to the stretching frequencies of ν(O–H) and ν(C=N) respectively. The two ν(C–O) bands for C–OH and C–OMe are observed at 1260 and 1086 cm^{-1} respectively.[42] In the complex, a distinct band appears at 1634 cm^{-1} corresponding to the azomethine (C=N) functional group.[43] The lowering of the stretching frequency from 1660 to 1634 cm^{-1} indicates the coordination to the metal center. The ν(C–O) band is shifted to 1217 cm^{-1} on complexation. Furthermore, the complex shows one sharp band at 2072 cm^{-1}, which indicates the presence of N_3 as a bridging ligand. Bands in agreement with the non-coordinated perchlorate anion could also be observed at 1110 cm^{-1} along with a weak shoulder at 629 cm^{-1}. The $\nu_{(M-N)}$ and $\nu_{(M-O)}$ stretching frequencies are observed at 462, 339 and 278 cm^{-1}.

Crystal structure

The molecular structure of the dinuclear nickel compound $[Ni(L)(\mu 1,1\text{-}N_3)Ni(L)(OH_2)_2]ClO_4{\cdot}2H_2O$ (**1**) is shown in Fig. 1 (for the ORTEP view with the complete labeling scheme see ESI, Fig. S2†). Relevant bond lengths and angles are given in Table 2. The cationic complex comprises two nickel(II) ions, two monodeprotonated [2-[{[2-(dimethylamino)ethyl]imino}-methyl]-6-methoxyphenol] ligands (tagged with labels A and B) roughly perpendicular to each other, a bridging azide anion and two water molecules.

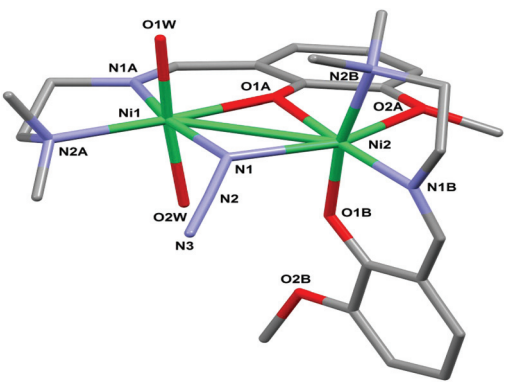

Fig. 1 Molecular structure of the cationic complex **1** with a partial labeling scheme. The perchlorate anion and the lattice water molecules have been omitted for clarity. The two ligands are tagged with labels A and B.

Table 2 Selected bond lengths [Å] and angles [°] for complex **1**

Ni1–O1A	1.997(4)	Ni2–O1B	2.005(3)	N2A–Ni1–O1A	173.29(9)
Ni1–N1A	2.020(8)	Ni2–N1B	1.999(6)	N1A–Ni1–N1	167.37(9)
Ni1–N2A	2.129(7)	Ni2–N2B	2.156(4)	O1W–Ni1–O2W	173.89(9)
Ni1–N1	2.117(5)	Ni2–N1	2.145(5)	N2B–Ni2–O1B	170.42(9)
Ni1–O1W	2.116(4)	Ni2–O1A	2.000(5)	O2A–Ni2–N1	153.10(9)
Ni1–O2W	2.119(4)	Ni2–O2A	2.275(5)	N1B–Ni2–O1A	174.80(9)
Ni1–Ni2	3.168(2)	Ni1–N1–Ni2	96.04(9)	Ni1–O1A–Ni2	104.87(9)

The dimer is assembled *via* the μ_2-nitrogen atom N1 of the azide anion and the μ_2-oxygen atom O1A of ligand A. Each metal center is in an octahedral NiN_3O_3 environment (more distorted for Ni2) but provided by a different set of ligands. Indeed, in the case of Ni1, only the Schiff base A is involved in the coordination; the equatorial plane is occupied by the imino and amino nitrogen atoms N1A and N2A, by the bridging nitrogen atom N1 of the azide anion and by the bridging phenolato oxygen O1A. The coordination is completed by two water oxygen atoms in the apical position. Ni2, which, in contrast, does not coordinate any water molecule, is chelated by both ligands A and B. In particular, considering the plane passing through ligand A as the equatorial plane, the metal center is surrounded by the bridging atoms O1A and N1, by the methoxy oxygen atom O2A and by the imino nitrogen atom N1B. In this case the apical positions are this time occupied by the amino nitrogen N2B and by the phenolate oxygen O1B. The potentially coordinating oxygen O2B remains dangling without taking part in any interaction.

The crystal structure is stabilized by a network of hydrogen bonds (relevant geometrical parameters are reported in Table 3) comprising the perchlorate anion, the coordinated and lattice water molecules, and the azide ligand. In particular, the complexes form a 1D supramolecular chain along the *b* direction of the unit cell through the O2W···N3 H-bond, involving one of the water molecules coordinated to Ni1 and the terminal nitrogen atom of the azide ligand bridging the two nickel centers (see Fig. 2). These chains are in turn connected by means of the hydrogen bonds involving the coordinated water molecule O1W, the lattice water molecules O3W and O4W, and the perchlorate anion (Fig. 3).

Table 3 Relevant geometrical parameters for the hydrogen bonds in complex **1**

O2W···N3	2.99(1)	O1···O3W	2.78(2)
O1W···O3W	2.86(1)	O4···O4W	2.35(2)
O1W···O4W	2.75(1)		

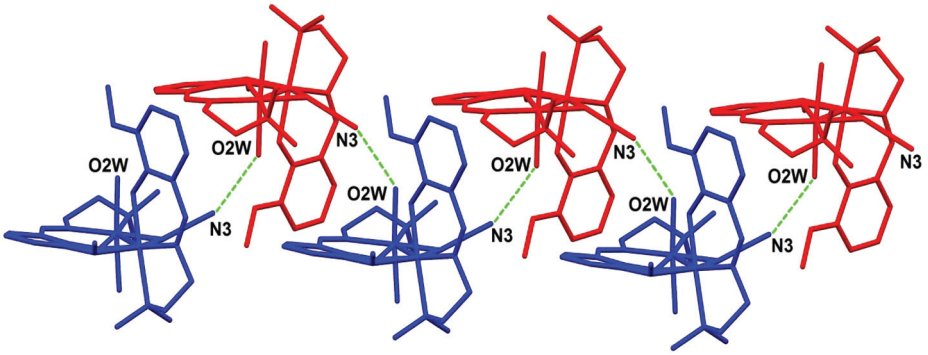

Fig. 2 Representation of the 1D supramolecular chain formed through H-bond interactions (green dotted lines) between the water oxygen O2W and the azide nitrogen N3.

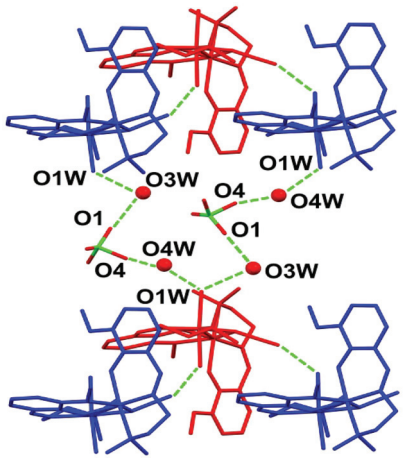

Fig. 3 The network of hydrogen bonds connecting the adjacent chains in the lattice.

Electronic spectra

The peaks in the electronic spectrum of complex **1** in methanol are similar, exhibiting d–d maxima typical of octahedral Ni^{II}.[44] In the ligand, the maximum absorption bands are ascertained to be at 232 and 315 nm which may arise due to $\pi \rightarrow \pi^*$ and $n \rightarrow \pi^*$ transitions. On complexation, the corresponding $\pi \rightarrow \pi^*$ and $n \rightarrow \pi^*$ bands are shifted from 235 to 282 nm and 315 to 382 nm, respectively (see ESI, Fig. S3†). The characteristic d–d band for a Ni(II) complex is recognised at 410 and 635 nm.

The spectral properties are explained by the DFT computation of the optimized structure of complex **1**. The orbital energies along with the contributions from the ligands and the metal for selected MOs are given in Fig. 4 (see details in the ESI, Table S1†). Although the orbital contribution of the ligands (L and H_2O) predominates in most cases in both filled and vacant MOs LUMO+1, LUMO+8 and HOMO−10 show a higher metal contribution. In the complex, it is observed that the occupied MOs HOMO, HOMO−3 and HOMO−6 and the unoccupied MOs from LUMO+3 to LUMO+7 all have more than 60% ligand contribution. Similarly, also the water contribution is significant in complex **1**, being ~60% for the MOs HOMO−1, HOMO−2, HOMO−4, HOMO−5 and LUMO. The contribution of the bridging ligand azide is almost insignificant in both occupied and unoccupied MOs with the exception of LUMO+9 which contains 60% azide function. In the complex, Ni contributes in an irregular fashion: 7% to HOMO, 15% to HOMO−1, 16% to HOMO−3, 8% to HOMO−7, 44% to HOMO−11 and 8% to LUMO, 42% to LUMO+1, 38% to LUMO+2, 38% to LUMO+3, 60% to LUMO+8 *etc*. Thus it is the ligands L and H_2O that mainly control the molecular orbitals and hence the spectral properties of the complex. Therefore HOMO → LUMO is considered as $L(\pi) \rightarrow H_2O(\pi^*)$; HOMO−3 → LUMO+3 is LLCT involving the L function ($L(\pi) \rightarrow L(\pi^*)$) whereas HOMO−1 → LUMO+8 is designated as the LMCT transition ($H_2O(\pi) \rightarrow Ni(d\pi)$) and HOMO−11 → LUMO is designated as MLCT ($Ni(d\pi) \rightarrow H_2O(\pi^*)$). The calculated transitions are grouped in Table 4. The intensity of these transitions has been assessed from the oscillator strength (f). In methanol, the longest wavelength band calculated at >650 nm (f, 0.0100) for **1** is assigned to the $Ni(d\pi) \rightarrow H_2O(\pi^*)$ transition followed by a highly intense transition at 411 nm (f, 0.0102) which is LLCT ($L(\pi) \rightarrow L(\pi^*)$) in nature. The other bands at 385 and 283 nm are LLCT in character whereas the high intensity band at 234 nm (f, 0.1510) is attributed to the $H_2O(\pi) \rightarrow Ni(d\pi)$ transition.

Emission spectra

Fluorescence studies of the ligand HL and complex **1** were carried out in methanol and the corresponding diagram is shown in Fig. 5. The emission bands of HL are observed at 364 and 423–445 nm upon exciting the $\pi \rightarrow \pi^*$ band while the maximum emission is found at 423 nm upon excitation at 315 nm. Complex **1** exhibits very low fluorescence efficiency when it is excited at the $\pi \rightarrow \pi^*$ transition and the maximum intensity occurs at 419 nm for λ_{ex} = 281 nm. No emission bands are detected at higher wavelength (>400 nm). The fluorescence quantum yield of the ligand and the complex was determined using carbazole as the reference with a known

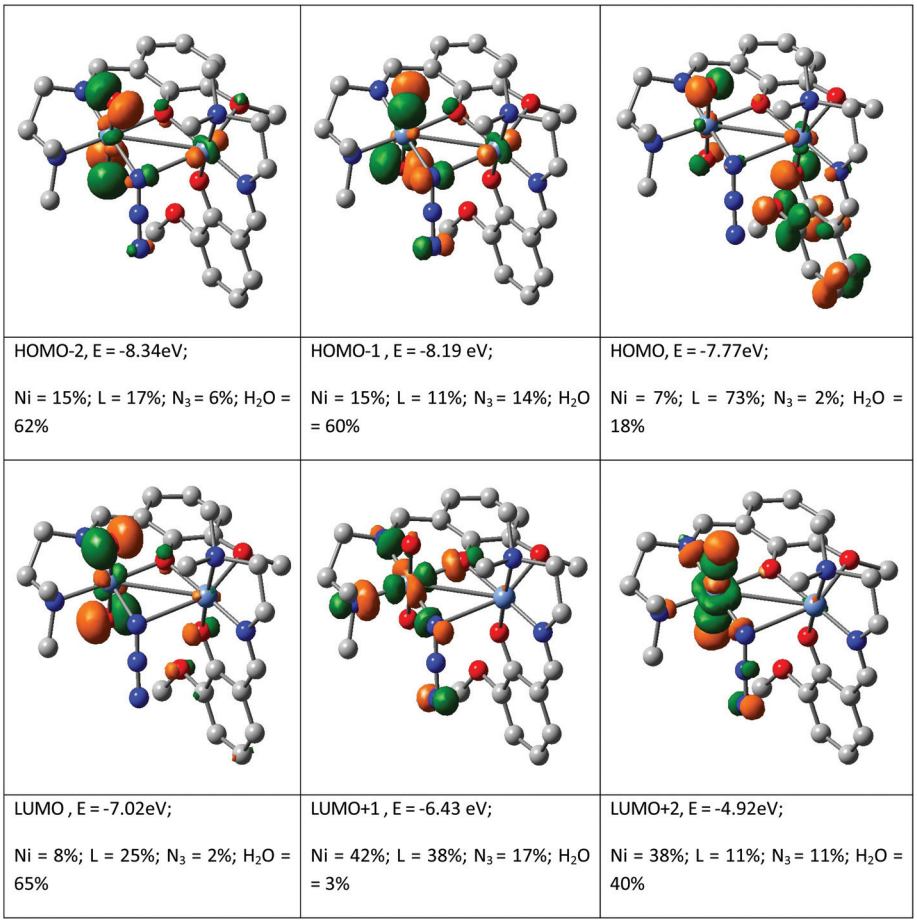

Fig. 4 Contour plots of some selected MOs of $[Ni(L)(\mu_{1,1}N_3)Ni(L)(OH_2)_2]\cdot ClO_4$.

Table 4 TD-DFT data of $[Ni(L)(\mu_{1,1}\text{-}N_3)Ni(L)(OH_2)_2]\cdot ClO_4$ [a]

Excitation energy (eV)	Wavelength (nm)	f	Key transitions	Character	Assignment
1.9019	651.90	0.0100	(32%) HOMO−11 → LUMO	Ni(dπ) → $H_2O(\pi^*)$	MLCT
3.0144	411.31	0.0102	(62%) HOMO → LUMO+5	L(π) → L(π*)	LLCT
3.2141	385.75	0.0134	(30%) HOMO−3 → LUMO+3	L(π) → L(π*)	LLCT
3.8999	317.92	0.0690	(18%) HOMO−7 → LUMO+3	$H_2O(\pi)$ → L(π*)	LLCT
4.3694	283.76	0.0152	(68%) HOMO−13 → LUMO+2	L(π) → $H_2O(\pi^*)$	LLCT
5.2873	234.49	0.1510	(9%) HOMO−1 → LUMO+8	$H_2O(\pi)$ → Ni(dπ)	LMCT

[a] LLCT (L(π) → L(π*)); MLCT (metal to ligand charge transfer); LLCT (ligand to ligand charge transfer); LMCT (ligand to metal charge transfer).

quantum yield value in benzene (Φ_R = 0.42). The fluorescence quantum yield of the complex corresponds to a π → π* transition band at 281 nm which is lower (0.005) than that of the ligand (0.022). This indicates the presence of energy transfer between the metal ion and the fluorophore ligand which coincides with a strong quenching of fluorescence.[45]

EPR spectra

EPR spectra of the polycrystalline complex **1** were recorded at liquid nitrogen temperature (77 K) and room temperature (298 K). The spectra are shown in Fig. 6. Ni(II) has a d^8 configuration and its EPR spectra can be interpreted using an $S = 1$ spin Hamiltonian. Even if it does not possess a Kramer doublet as the lowest state in a magnetic field, usually spectra can be recorded for octahedral complexes.[46] The spectra reported in traces a and b of Fig. 6 can be interpreted with a nearly isotropic g tensor with g factors of 2.158 and 2.085 (298 K, trace a) and 2.182 and 2.080 (77 K, trace b), in agreement with the structure determined by X-ray diffraction analysis.

The EPR signal disappears almost completely when the solid complex **1** is dissolved in a coordinating solvent such as DMF (or DMSO, spectrum not shown) and in a weakly coordi-

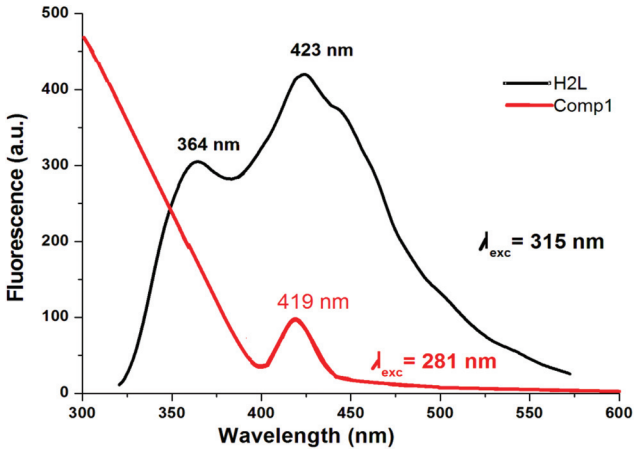

Fig. 5 Emission spectra of HL (black curve, in DMF) and of the Ni(II) complex (**1**) (red curve, in MeOH).

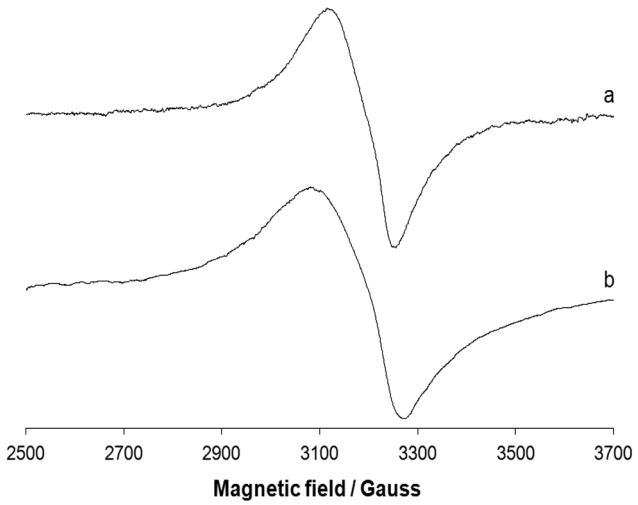

Fig. 6 X-band EPR spectra of the polycrystalline complex **1** at (a) 298 and (b) 77 K.

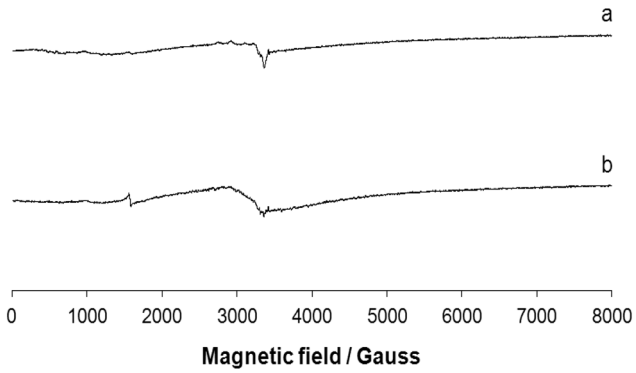

Fig. 7 Anisotropic X-band EPR spectra of the complex **1** dissolved in (a) DMF and (b) CH_3CN.

nating solvent such as CH_3CN (Fig. 7). This indicates a diamagnetic ground state with $S = 0$, which can be associated with a square planar geometry.[47] This means that in the presence of a coordinating solvent the two bridges are broken and mononuclear units are formed with the coordination of the tridentate ligand and a solvent molecule in the fourth equatorial position (Scheme 1). The tendency of polynuclear metal complexes to dissociate in solution is now a well-accepted fact in the literature and has been demonstrated in many cases, for example in the case of di- and polymeric Cu(II) species.[48]

Magnetic moment

The temperature variation of the magnetic properties (in the temperature range from 5 to 300 K under an external field of 10 000 Oe) of complex **1** in the form of a $\chi_m T$ *vs.* T (χ_m *vs.* T inset) plot is shown in Fig. 8 (χ_m is the molar susceptibility for two Ni(II) ions). At room temperature, the $\chi_m T$ value is 4.33 emu K G^{-1} mol^{-1}. When lowering the temperature, the $\chi_m T$ value increases gradually to a maximum value of 5.82 emu K G^{-1} mol^{-1} at 18 K. It then decreases sharply with decreasing temperature and reaches a minimum of 4.81 emu K G^{-1} mol^{-1} at 5 K. This behaviour suggests that there are ferromagnetic interactions between the bridging binuclear Ni(II) ions ($S = 1$), because of the super-exchange interaction.

Antimycobacterial activity

In the anti-mycobacterial assay, HL and complex **1** were tested against *M. tuberculosis* H37Rv and *M. tuberculosis* H37Ra strains as well as against two clinical strains (strain-1 and strain-2). The results are shown in Table 5. *M. tuberculosis* H37Rv and *M. tuberculosis* H37Ra, a well-known indicator, are used for the drug sensitivity tests.[12] The MIC and the MBC of HL for *M. tuberculosis* $H_{37}Rv$ are 4 and 8 μg mL^{-1}, while the MIC and MBC of complex **1** are 8 μg mL^{-1}. Although HL shows the same MIC value against *M. tuberculosis* $H_{37}Rv$ and *M. tuberculosis* $H_{37}Ra$, the MBC value against *M. tuberculosis* $H_{37}Ra$ is higher than that against *M. tuberculosis* $H_{37}Rv$. On the other hand, the highest MIC and MBC values in the clinical isolates have been found for strain-1 (MIC 16 μg mL^{-1} and MBC 32 μg mL^{-1}) in the case of HL and for strain-2 (MIC 32 μg mL^{-1} and MBC 64 μg mL^{-1}) in the case of complex **1**. The results show that the compounds exhibit antimycobacterial activity against the tested drug resistant and drug susceptible *M. tuberculosis* strains with MIC at 4 μg ml^{-1} and MBC in the range of 8–16 μg mL^{-1}. Clinical strains are also affected by the compounds with MIC 8–32 μg mL^{-1} and MBC 16–64 μg mL^{-1} (Table 5). Both HL and complex **1** show bactericidal activity. The ligand HL is more effective against drug resistant and drug susceptible *M. tuberculosis* and clinical isolates than complex **1** (Fig. 9). In this study, we state that both compounds show a considerable efficacy on the mycobacterial strains. The mycobacterial cell wall includes a large amount of complex lipids, lipopolysaccharides and mycolic acids. This constitution makes the cell wall a strong hydrophobic barrier against antimicrobial agents.[49]

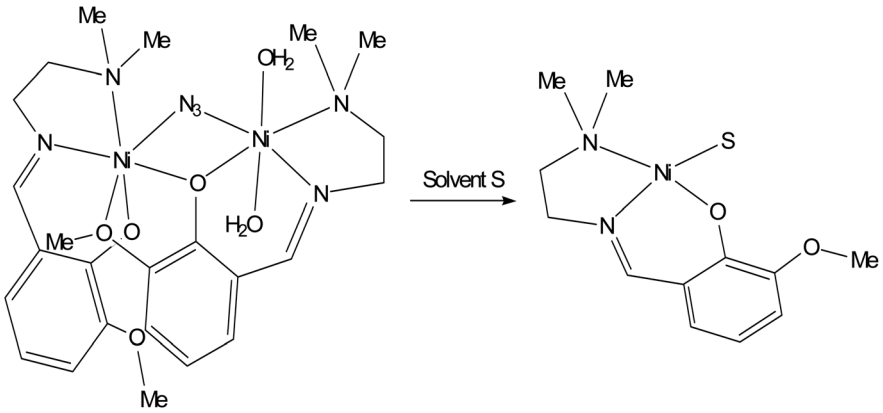

Scheme 1 Dissociation of complex **1** in the presence of a coordinating solvent S (S = DMF, DMSO, CH_3CN).

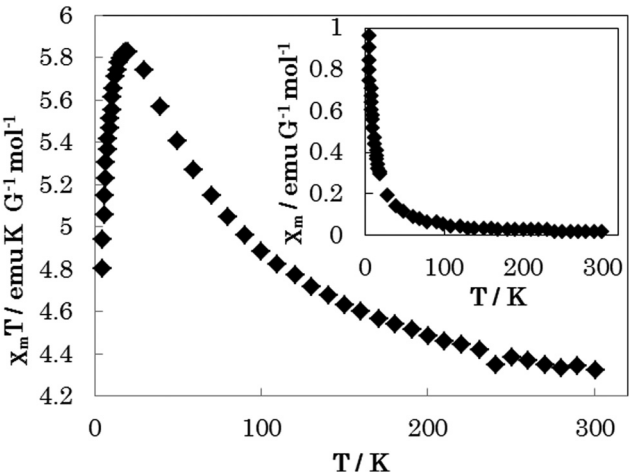

Fig. 8 The temperature-dependent magnetic susceptibility data for **1** were measured in the temperature range from 5 to 300 K under an external field of 10 000 Oe.

Cytotoxicity study

The ligand, HL, and complex **1** were investigated for cytotoxic effects on three cancer cell lines, namely A-549 (non-small cell lung cancer), MCF-7 (breast cancer), and CaCo-2 (colon cancer cell line), and on one healthy cell line, CRL-2522 (human normal fibroblast). Generally, cytotoxic effects of the substances increase in conjunction with an increase in concentration. While HL has 24.82 > 55.38 > 79.71 μg mL^{-1} downward IC_{50} values on CaCo-2 > A-549 > MCF-7 respectively, it has the highest IC_{50} value (306.75) on the healthy cell line CRL-2522 (see ESI, Table S2†). This result is desirable for drug

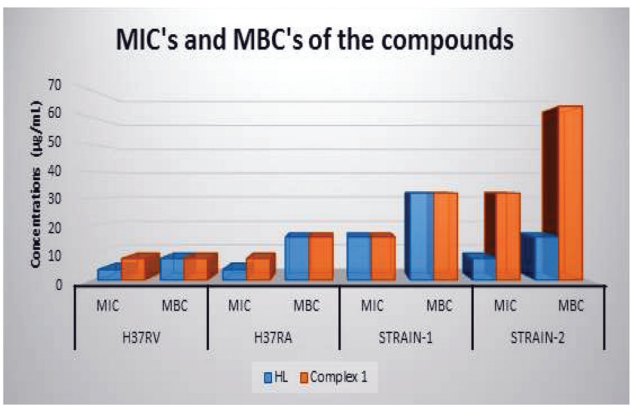

Fig. 9 MIC's and MBC's of HL and complex **1**.

Table 5 Minimal inhibitory concentration (MIC) and minimal bactericidal concentration (MBC) of HL and complex **1** (μg mL^{-1})

	Bacteria							
	Drug resistant and drug susceptible *M. tuberculosis*				Clinical isolates			
	$H_{37}Rv$		$H_{37}Ra$		Strain-1		Strain-2	
Compounds	MIC	MBC	MIC	MBC	MIC	MBC	MIC	MBC
HL	4	8	4	16	16	32	8	16
Complex **1**	8	8	8	16	16	32	32	64
Concentrations of antimycobacterial drugs (μg mL^{-1})								
Streptomycin	0.65	0.65	0.65	1.29	2.59	5.18	0.65	—
Isoniazid	0.13	1.03	0.51	1.03	0.51	1.03	0.51	0.51
Rifampicin	0.65	5.18	0.32	2.59	0.65	0.65	0.65	5.18
Ethambutol	3.744	7.48	1.87	1.87	3.74	3.74	1.87	—

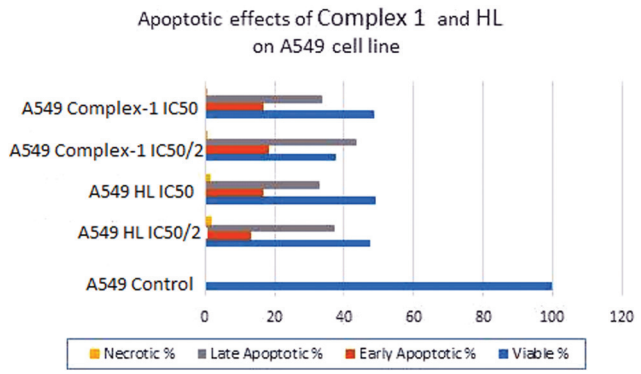

Fig. 10 The ligand HL and complex **1** induced apoptosis in A-549 cells in a concentration-dependent fashion. In the case of MCF-7, Caco-2 and CRL-2522 cell lines, minimum apoptotic effects are obtained (data not shown).

development methods and for that reason, HL is a candidate molecule for target drugs. CRL-2522 (human normal fibroblast) shows an apoptotic effect under 1% at both IC_{50} and $IC_{50/2}$ concentrations (Fig. 10).

Apoptosis detection by staining with Annexin V-fluorescein isothiocyanate and propidium iodide (FACS)

To determine and measure apoptotic events, the expression of phosphatidylserine at the cell surface is effected by flow cytometry (FCM) with Annexin-V-fluorescein isothiocyanate (FITC) and propidium iodide (PI). To study late apoptotic events, DNA strand breaks are determined compared with the PI.[50] The early apoptotic cells were Annexin V-positive and PI-negative, and the late apoptotic and dead cells were Annexin V-positive and PI-positive.[51] In the IC_{50} and $IC_{50/2}$ concentrations of complex **1**, the total apoptosis rate exceeds 50% on the A-549 cell line. The MTT analysis indicates that complex **1** represses cell proliferation in a dose-subordinate procedure and this is confirmed by flow cytometric experiments using Annexin V–PI. The highest apoptotic rate is observed after treatment with complex **1** at $IC_{50/2}$ (21.05 μg mL^{-1}). Circumstantially, the higher dosages (IC_{50}) of complex **1** (42.301 μg mL^{-1}) result in relatively lower apoptotic rates (see ESI, Table S3†). CRL-2522 (human normal fibroblast) shows an apoptotic effect under 1% at both IC_{50} and $IC_{50/2}$ concentrations. Complex **1** could be considered the best candidate for a drug active material since it needs a minimum concentration level to show cytotoxic activity on three cancer lines and is non-toxic even at high concentrations on the healthy cell line fibroblast.

Docking study with enoyl acyl carrier protein reductase of *M. tuberculosis* H37Rv

InhA, the enoyl acyl carrier protein reductase (ENR) from *M. tuberculosis*, is one of the key enzymes involved in the mycobacterial fatty acid elongation cycle and has been validated as an effective antimicrobial target. Isoniazid is a well-known tuberculosis drug that binds in the pocket of enoyl acyl carrier protein reductase and inhibits the action of fatty acid synthase. Pyrrolidine carboxamides[52] are reported as a novel class of potent InhA inhibitors. By theoretical calculation we have tried to establish whether the ligand HL can act as a new InhA inhibitor. The crystallographic structures of the enoyl acyl carrier protein reductase of *M. tuberculosis* $H37R_v$ and of the pyrollidium carboxamide complex were downloaded from the RCSB protein data bank (PDB ID: 4U0K); they were resolved at 1.09 Å using X-ray diffraction analysis. The energy-minimized structure of the ligand was used *in situ* for the protein–ligand docking studies in the cavity of the enzyme. To perform the docking study with HL and the enoyl acyl carrier protein reductase, we have selected the binding cavity of pyrollidium carboxamides. A total of fourteen amino acids (Ile21, Gly96, Phe97, Met98, Met103, Met147, Asp148, Phe149, Tyr158, Met161, Lys165, Ala193, Pro193, Met199) were present in the cavity sites. The ligand HL interacts with the protein forming two hydrogen bonds with Lys165 (1.94 and 2.53 Å, Fig. 11 and 12). The relevant data of the docking study are given in

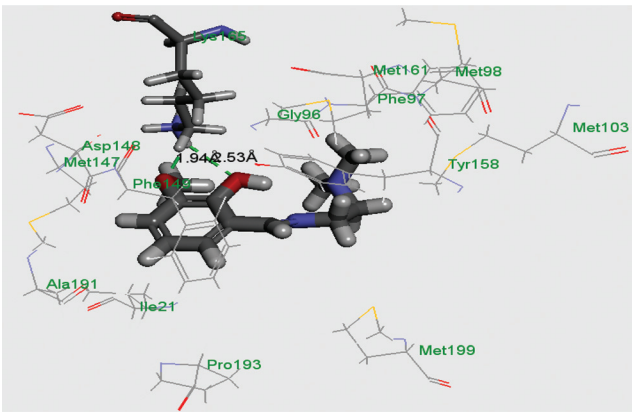

Fig. 11 Best docked pose of the ligand (HL) inside the binding pocket of enoyl acyl carrier protein reductase (PDB id 4U0K) of *M. tuberculosis* $H37R_v$ (2D view).

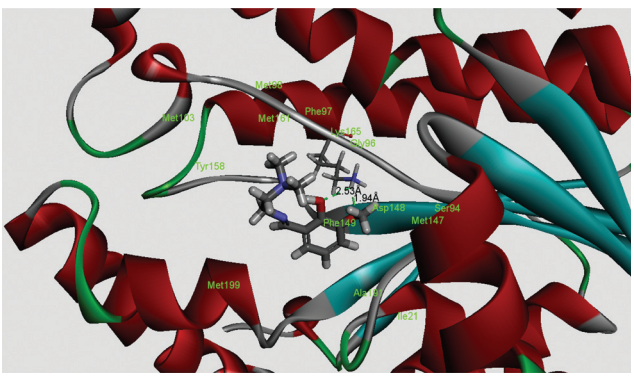

Fig. 12 Best docked pose of the ligand (HL) (3D view) and the enoyl acyl carrier protein reductase (PDB id 4U0K) of *M. tuberculosis* $H37R_v$ (3D view).

Table 6 Details of the docking studies[a]

Compound	CDOCKER interaction energy	Energy of the protein–molecule complex (kcal mol^{-1})	Ligand energy (kcal mol^{-1})	Protein energy (kcal mol^{-1})	Binding energy (kcal mol^{-1})
4U0K@HL	−17.46	−10 299.00	23.86	−10 272.18	−50.67
4U0K@pyrollidium carboxamides	−22.76	−10 324.26	−12.58	−10 272.18	−39.50

[a] $Energy_{Binding} = Energy_{Complex} - Energy_{Ligand} - Energy_{Receptor}$.

Table 7 Details of the interactions present in the most stable protein–ligand complex

	Hydrogen bonds				
Compounds	No. of hydrogen bonds	End 1	End 2	Bond distances (Å)	Angle DHA
HL	2	Lys165	O-Atom of the phenolic group	2.63	132.19
		Lys165	O-Atom of the methoxy group	1.94	126.43
Pyrollidium carboxamides	1	Tyr158	O-Atom of carbonyl carbon	1.93	164.5

Tables 6 and 7. The surface area of the active site cavity (with respect to the H-bond donors/acceptors) is depicted in Fig. 13. We have removed the pyrollidium carboxamides from the binding cavity and docked inside the cavity. The best docked pose of the enoyl acyl carrier protein reductase and of pyrollidium carboxamides is comparable to the reported crystal data (4U0K) (see ESI, Fig. S4†). We have compared the Gibbs free energies of the protein–molecule complex for pyrollidium carboxamides and the ligand, HL. The protein–molecule complex for pyrollidium carboxamide is slightly more stable than the complex with the ligand (Table 6).

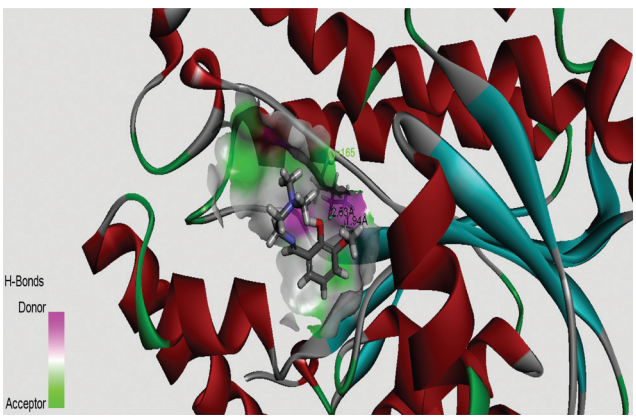

Fig. 13 Surface area (with respect to the H-bond donors & acceptors) of the binding pocket in the best docked pose of the ligand and protein.

Druglikeness and ADMET prediction

Druglikeness and ADMET properties of HL have been checked following Lipinski's rule of five and the ADMET prediction module of Discovery Studio 4.0. The ligand has passed Lipinski's filter, and according to the ADMET (absorption, distribution, metabolism, excretion and toxicity) prediction it is non-mutagenic and shows optimal druglikeness. Predicted data are summarized in Table 8.

Conclusions

A potential tetradentate monoanionic N_2O_2 chelator, HL, is synthesized which affords the corresponding nickel derivative, $[Ni(L)(\mu_{1,1}\text{-}N_3)Ni(L)(OH_2)_2]\cdot ClO_4$ (**1**) (HL, [2-[{[2-(dimethylamino)ethyl]imino}methyl]-6-methoxyphenol]) when reacting with nickel perchlorate and sodium azide. The solid state structure of **1** shows that both the Ni atoms possess an octahedral N_3O_3 environment. The complex has been thoroughly

Table 8 ADMET prediction for HL[a]

Compounds	Molecular weight	ADMET solubility (aqueous)	ADMET solubility level	ADMET absorption level[a]	ADMET_A log *P*98	No of H-bond acceptors	No. of H-bond donors	Lipinski's filter	Drug likeness inference	Ames prediction
HL	222.84	−1.886	4	0 (good)	1.73	4	1	Yes	Yes, optimal	Non-mutagen

[a] ADMET absorption level: 0, good; 1, moderate; 2, low.

characterized by means of different spectral analyses. The temperature dependent magnetic moment shows the existence of ferromagnetic interactions between the bridging dinuclear Ni(II) ions. Both the ligand HL and complex **1** exhibit moderate anti-mycobacterial activity and considerable efficacy on the *M. tuberculosis* H37Rv ATCC 27294 and *M. tuberculosis* H37Ra ATCC 25177 strains. As regards the cytotoxicity study, it has been proven that both the ligand and the complex respond well on cancer cell lines (A-549, MCF-7 and Caco-2); however complex **1** shows low toxicity on healthy cell lines like CRL-2522. Further investigations in this area involving other metal ions integrated with new organic precursors and considering the chemo-sensor activities of the ligands for selective detection of metal ions are currently being carried out in our laboratories.

Acknowledgements

KD and CS would like to thank West Bengal DST, Kolkata, India for the grant (228/1(10)/(Sanc.)/ST/P/S&T/9G-16/2012). AD would like to thank The National Science Council, Taiwan for financial assistance. We also thank Mr Kana Kobayashi for his valuable suggestions regarding the magnetic studies.

References

1 (*a*) P. Zanello, S. Tamburini, P. A. Vigato and G. A. Mazzochim, *Coord. Chem. Rev.*, 1987, **77**, 165–273; (*b*) P. A. Vigato, S. Tamburini and D. E. Fenton, *Coord. Chem. Rev.*, 1990, **106**, 25–170; (*c*) G. A. Morris, H. Zhou, C. L. Stern and S. T. Nguyen, *Inorg. Chem.*, 2001, **40**, 3222–3227; (*d*) N. N. Murthy, M. M. Tahir and K. D. Karlin, *J. Am. Chem. Soc.*, 1993, **115**, 10404–10405; (*e*) K. Bertoncello, G. D. Fallon, J. H. Hodgkin and K. S. Murray, *Inorg. Chem.*, 1988, **27**, 4750–4758; (*f*) N. R. Sangeetha, C. K. Pal, P. Ghosh and S. Pal, *J. Chem. Soc., Dalton Trans.*, 1996, 3293–3296; (*g*) N. R. Sangeetha, K. Baradi, R. Gupta, C. K. Pal, V. Manivannan and S. Pal, *Polyhedron*, 1999, **18**, 1425–1429.

2 (*a*) S. H. Strauss, *Chem. Rev.*, 1993, **93**, 927–942; (*b*) S. O. Kang, R. A. Begum and K. Bowman-James, *Angew. Chem., Int. Ed.*, 2006, **45**, 7882–7884; (*c*) J. H. Han, J. W. Shin and K. S. Min, *Bull. Korean Chem. Soc.*, 2009, **30**, 1113–1117.

3 (*a*) S. K. Dey, N. Mondal, M. S. El Fallah, R. Vicente, A. Escuer, X. Solans, M. F. Bardia, T. Matsushita, V. Gramlich and S. Mitra, *Inorg. Chem.*, 2004, **43**, 2427–2434; (*b*) P. Talukder, A. Datta, S. Mitra, G. Rosair, M. S. El Fallah and J. Ribas, *Dalton Trans.*, 2004, 4161–4167; (*c*) N. K. Karan, S. Mitra, T. Matsushita, V. Gramlich and G. Rosair, *Inorg. Chim. Acta*, 2002, **332**, 87–91.

4 (*a*) S. Naiya, C. Biswas, M. G. B. Drew, C. J. Gómez-Garcıa, J. M. Clemente-Juan and A. Ghosh, *Inorg. Chem.*, 2010, **49**, 6616–6627; (*b*) O. Sengupta and P. S. Mukherjee, *Inorg. Chem.*, 2010, **49**, 8583–8590; (*c*) O. Sengupta, G. Bappaditya, S. Mukherjee and P. S. Mukherjee, *Dalton Trans.*, 2010, **39**, 7451–7465; (*d*) K. C. Mondal, M. G. B. Drew and P. S. Mukherjee, *Inorg. Chem.*, 2007, **46**, 5625–5629.

5 E. Ruiz, J. Cano, S. Alvarez and P. Alemany, *J. Am. Chem. Soc.*, 1998, **120**, 11122–11129.

6 (*a*) C. P. Landee and R. D. Willett, *Inorg. Chem.*, 1981, **20**, 2521–2525; (*b*) J. C. Jansen, H. van Koningsveld, J. A. C. vah Ooijen and J. Reedijk, *Inorg. Chem.*, 1980, **19**, 170–174; (*c*) R. J. Butcher and E. Sinn, *Inorg. Chem.*, 1977, **16**, 2334–2343; (*d*) H. S. Preston and C. H. L. Kennard, *J. Chem. Soc. A*, 1969, 2682–2686.

7 (*a*) A. P. Ginsberg, R. L. Martin, R. W. Brookes and R. C. Sherwood, *Inorg. Chem.*, 1972, **11**, 2884–2889; (*b*) T. Rojo, L. Lezama, R. Cortes, J. L. Mesa, M. I. Arriortua and G. Villeneuve, *J. Magn. Magn. Mater.*, 1990, **83**, 519–521.

8 O. Kahn, *Inorg. Chim. Acta*, 1982, **62**, 3–14.

9 (*a*) N. Mondal, S. Mitra, V. Gramlich, S. O. Ghodsi and K. M. A. Malik, *Polyhedron*, 2001, **20**, 135–141; (*b*) M. Amirnasr, K. J. Schenk, S. Meghdadi and M. Morshedi, *Polyhedron*, 2006, **25**, 671–677.

10 A. L. Okunade and M. P. F. Elvin-Lewis, *Phytochemistry*, 2004, **65**, 1017–1032.

11 N. Lall, M. D. Sarma, B. Hazra and J. J. Meyer, *J. Antimicrob. Chemother.*, 2003, **51**, 435–438.

12 E. Banfi, M. G. Mamolo, D. Zampieri, L. Vio and C. M. Bragadin, *J. Antimicrob. Chemother.*, 2001, **48**, 705–711.

13 E. Vattemi and P. P. Claudio, *Drug News Perspect.*, 2007, **20**, 511–520.

14 K. C. Zimmermann, C. Bonzon and D. R. Green, *Pharmacol. Ther.*, 2001, **92**, 57–70.

15 (*a*) N. A. Thornberry, T. A. Rano, E. P. Peterson, D. M. Rasper, T. Timkey, M. Garcia-Calvo, V. M. Houtzager, P. A. Nordstrom, S. Roy, J. P. Vaillancourt, K. T. Chapman and D. W. Nicholson, *J. Biol. Chem.*, 1997, **272**, 17907–17911; (*b*) A. Marin-Hernandez, I. Gracia-Mora, L. Ruiz-Ramirez and R. Moreno-Sanchez, *Biochem. Pharmacol.*, 2003, **65**, 1979–1989.

16 R. Koner, S. Hazra, M. Fleck, A. Jana, C. R. Lucas and S. Mohanta, *Eur. J. Inorg. Chem.*, 2009, 4982–4988.

17 (*a*) S. Sen, P. Talukder, S. K. Dey, S. Mitra, G. Rosair, D. L. Hughes, G. P. A. Yap, G. Pilet, V. Gramlich and T. Matsushita, *Dalton Trans.*, 2006, 1758–1767; (*b*) S. Basak, S. Sen, S. Banerjee, S. Mitra, G. Rosair and M. T. G. Rodriguez, *Polyhedron*, 2007, **26**, 5104–5112; (*c*) C. R. Choudhury, S. K. Dey, R. Karmakar, C.-D. Wu, C.-Z. Lu, M. S. El Fallah and S. Mitra, *New J. Chem.*, 2003, **27**, 1360–1366; (*d*) G. Das, R. Shukla, S. Mandal, R. Singh and P. K. Bharadwaz, *Inorg. Chem.*, 1997, **36**, 323–329.

18 D. F. Eaten, *Pure Appl. Chem.*, 1988, **60**, 1107–1114.

19 S. R. Stoyanov, J. M. Villegas and D. P. Rillema, *Inorg. Chem.*, 2002, **41**, 2941–2945.

20 (*a*) *SADABS Bruker AXS*, Madison, Wisconsin, USA, 2004; *SAINT, Software Users Guide, Version 6.0*, Bruker Analytical X-ray Systems, Madison, WI, 1999(*b*) G. M. Sheldrick, *SADABS v2.03: Area-Detector Absorption Correction*, University of Göttingen, Germany, 1999.
21 A. Altomare, M. C. Burla, M. Camalli, G. L. Cascarano, C. Giacovazzo, A. Guagliardi, A. G. G. Moliterni, G. Polidori and R. Spagna, *J. Appl. Crystallogr.*, 1999, **32**, 115–119.
22 G. M. Sheldrick, *Acta Crystallogr., Sect. A: Fundam. Crystallogr.*, 2008, **64**, 112–122.
23 L. J. Farrugia, *J. Appl. Crystallogr.*, 1999, **32**, 837–838.
24 C. Lee, W. Yang and R. G. Parr, *Phys. Rev. B: Condens. Matter*, 1988, **37**, 785–789.
25 M. J. Frisch, G. W. Trucks, H. B. Schlegel, G. E. Scuseria, M. A. Robb, J. R. Cheeseman, J. A. Montgomery Jr., T. Vreven, K. N. Kudin, J. C. Burant, J. M. Millam, S. S. Iyengar, J. Tomasi, V. Barone, B. Mennucci, M. Cossi, G. Scalmani, N. Rega, G. A. Petersson, H. Nakatsuji, M. Hada, M. Ehara, K. Toyota, R. Fukuda, J. Hasegawa, M. Ishida, T. Nakajima, Y. Honda, O. Kitao, H. Nakai, M. Klene, X. Li, J. E. Knox, H. P. Hratchian, J. B. Cross, V. Bakken, C. Adamo, J. Jaramillo, R. Gomperts, R. E. Stratmann, O. Yazyev, A. J. Austin, R. Cammi, C. Pomelli, J. W. Ochterski, P. Y. Ayala, K. Morokuma, G. A. Voth, P. Salvador, J. J. Dannenberg, V. G. Zakrzewski, S. Dapprich, A. D. Daniels, M. C. Strain, O. Farkas, D. K. Malick, A. D. Rabuck, K. Raghavachari, J. B. Foresman, J. V. Ortiz, Q. Cui, A. G. Baboul, S. Clifford, J. Cioslowski, B. B. Stefanov, G. Liu, A. Liashenko, P. Piskorz, I. Komaromi, R. L. Martin, D. J. Fox, T. Keith, M. A. Al-Laham, C. Y. Peng, A. Nanayakkara, M. Challacombe, P. M. W. Gill, B. Johnson, W. Chen, M. W. Wong, C. Gonzalez and J. A. Pople, *GAUSSIAN 03 Revision D 01*, Gaussian Inc., Wallingford, CT, 2004.
26 *GaussView3.0*, Gaussian, Pittsburgh, PA.
27 P. J. Hay and W. R. Wadt, *J. Chem. Phys.*, 1985, **82**, 270–283.
28 R. Bauernschmitt and R. Ahlrichs, *Chem. Phys. Lett.*, 1996, **256**, 454–464.
29 M. K. Casida, C. Jamorski, K. C. Casida and D. R. Salahub, *J. Chem. Phys.*, 1998, **108**, 4439–4449.
30 R. E. Stratmann, G. E. Scuseria and M. J. Frisch, *J. Chem. Phys.*, 1998, **109**, 8218–8224.
31 M. Cossi, N. Rega, G. Scalmani and V. Barone, *Comput. Chem.*, 2003, **24**, 669–681.
32 N. M. O'Boyle, A. L. Tenderholt and K. M. Langner, *J. Comput. Chem.*, 2008, **29**, 839–845.
33 B. D. Becton, Dickinson and Company Newsletter BD Bactec MGIT 960 SIRE kit now FDA-cleared for susceptibility testing of *Mycobacterium tuberculosis*. Microbiology News & Ideas 13: 4-4, 2002.
34 NCCLS (2003). National Committee for Clinical Laboratory Standards (NCCLS). Susceptibility Testing of Mycobacteria, Nocardiae, and Other Aerobic Actinomycetes; Approved Standard. NCCLS document M24-A [ISBN 1-56238-500-3]. NCCLS, 940 West Valley Road, Suite 1400, Wayne, Pennsylvania 19087-1898, USA, 2003.
35 L. Collins and S. G. Franzblau, *Antimicrob. Agents Chemother.*, 1997, **41**, 1004–1009.
36 A. Jimenez-Arellanes, M. Meckes, R. Ramirez, J. Torres and J. Luna-Herrera, *Phytother. Res.*, 2003, **17**, 903–908.
37 (*a*) G. R. Battu and B. M. Kumar, *Willd. Pharmacogn. J.*, 2010, **2**, 456–463; (*b*) P. Bontempo, V. Carafa, R. Grassi, A. Basile, G. C. Tenore, C. Formisano, D. Rigano and L. Altucci, *Food Chem. Toxicol.*, 2013, 304–312.
38 T. Mosman, *J. Immunol. Methods*, 1983, **65**, 55–63.
39 C. A. Lipinski, F. Lombardo, B. W. Dominy and P. J. Feeney, *Adv. Drug Delivery Rev.*, 2001, **46**, 3–26.
40 C. A. Lipinski, *Drug Discovery Today: Technol.*, 2004, **1**, 337–341.
41 Discovery Studio 4.0 is a product of Accelrys Inc., San Diego, CA, USA.
42 K. Nakamoto, *Infrared and Raman Spectra of Inorganic and Coordination Compounds, Parts A and B*, John Wiley, New York, 5th edn, 1997.
43 S. Ferrer, J. G. Haasnoot, J. Reedijk, E. Muller, M. B. Cingi, M. Lanfranchi, A. M. M. Lanfredi and J. Ribas, *Inorg. Chem.*, 2000, **39**, 1859–1867.
44 A. B. P. Lever, *Inorganic Electronic Spectroscopy*, Elsevier, New York, 2nd edn, 1984.
45 (*a*) J. L. Kropp and M. W. Windsor, *J. Chem. Phys.*, 1963, **39**, 2769–2770; (*b*) J. L. Kropp and M. W. Windsor, *J. Chem. Phys.*, 1965, **42**, 1599–1608.
46 A. Bencini and D. Gatteschi, in *Transition Metal Chemistry*, ed. G. A. Melson and B. N. Figgis, Marcel Dekker, New York, 1982, vol. 8, pp. 1–178.
47 F. A. Cotton, G. Wilkinson, C. A. Murillo and M. Bochmann, *Advanced Inorganic Chemistry*, John Wiley & Sons, Inc., New York, 6th edn, 1999.
48 (*a*) J. C. Jeffery, J. P. Maher, C. A. Otter, P. Thornton and M. D. Ward, *J. Chem. Soc., Dalton Trans.*, 1995, 819–824; (*b*) W. A. Alves, R. H. A. Santos, A. Paduan-Filho, C. C. Becerra, A. C. Borin and A. M. D. C. Ferreira, *Inorg. Chim. Acta*, 2004, **357**, 2269–2278; (*c*) M. A. Ali, A. H. Mirza, R. J. Fereday, R. J. Butcher, J. M. Fuller, S. C. Drew, L. R. Gahan, G. R. Hanson, B. Moubaraki and K. S. Murray, *Inorg. Chim. Acta*, 2005, **358**, 3937–3948; (*d*) I. A. Koval, M. Sgobba, M. Huisman, M. Lüken, E. Saint-Aman, P. Gamez, B. Krebs and J. Reedijk, *Inorg. Chim. Acta*, 2006, **359**, 4071–4078; (*e*) S. Thakurta, J. Chakraborty, G. Rosair, J. Tercero, M. S. El Fallah, E. Garribba and S. Mitra, *Inorg. Chem.*, 2008, **47**, 6227–6235; (*f*) S. Thakurta, P. Roy, G. Rosair, C. J. Gomez-Garcia, E. Garribba and S. Mitra, *Polyhedron*, 2009, **28**, 695–702; (*g*) S. Saha, A. Sasmal, C. R. Choudhury, C. J. Gomez-Garcia, E. Garribba and S. Mitra, *Polyhedron*, 2014, **69**, 262–269.
49 (*a*) D. E. Minnikin and M. Goodfellow, in *Microbiological classification and identification*, ed. R. G. Board, Academic, London, 1980, p. 189; (*b*) D. E. Minnikin, Lipids; complex lipids, their chemistry, biosynthesis and roles, in *The biology of mycobacteria*, ed. C. Ratledge and J. Stanford, Academic Press, Inc., London, 1982, p. 95.

50 M. Martinez-Losa, J. Cortijo, G. Juan, M. Ramón, M. J. Sanz and E. J. Morcillo, Modulatory effects of N-acetyl-L-cysteine on human eosinophil apoptosis, *ERJ*, 2007, **30**, 436.
51 T. Nakanoma, M. Ueno, M. Iida, R. Hirata and N. Deguchi, *Int. J. Urol.*, 2001, **8**, 623–630.
52 X. He, A. Alian, R. Stroud and P. R. Ortiz de Montellano, *J. Med. Chem.*, 2006, **49**, 6308–6323.